Journal of the European Ceramic Society 19 (1999) 317–327

PII: S0955-2219(98)00081-8
0955-2219/99/$—see front matter

Carbon Fiber-reinforced (YMAS) Glass-Ceramic Matrix Composites. III. Interfacial Aspects

Valérie Bianchi,[a] Paul Goursat,[a]* Wharton Sinkler,[b] Marc Monthioux[b] and Erik Ménessier[c]

[a]LMCTS, URA CNRS 320, Faculté des Sciences, 123, Avenue Albert Thomas, 87060 Limoges Cedex, France
[b]CEMES, UPR A-8011 CNRS, B.P. 4347, 31055 Toulouse Cedex, France
[c]Céramiques et Composites, B.P. 7, 65460 Bazet, France

(Received 12 May 1997; accepted 25 February 1998)

Abstract

Unidirectional continuous carbon fiber-reinforced glass-ceramic matrix composites have been fabricated for dry sliding applications. Different fracture behaviors have been observed (three-point bend test and fracture surfaces observation). Besides, the distance between next microcracks, which have appeared in the matrix on cooling after hot-pressing of the composites, changes with the sintering temperature, suggesting fiber–matrix reactions. The nature of the fiber–matrix interface is observed in Transmission Electronic Microscopy and the interfacial shear stress is determined by push-in tests. © *1998 Elsevier Science Limited. All rights reserved*

Résumé

Des composites unidirectionnels à fibres longues de carbone et matrice vitrocéramique ont été élaborés pour des applications en frottement sec. Différents comportements à la rupture ont été observés (essai en flexion trois points et observation des fractures). Par ailleurs, la distance séparant deux fissures voisines, apparues dans la matrice lors du refroidissement aprés le frittage sous charge, change avec la température de frittage, suggérant une réaction entre la fibre et la matrice. La nature de l'interface fibre-matrice est observeé en Microscopie Electronique en Transmission et la contrainte de cisaillement interfaciale est déterminee lors d'essais de micro-indentation des fibres.

Keywords: mechanical properties, glass ceramics, composites, carbon fibres, interfaces.

*To whom correspondence should be addressed.

1 Introduction

The use of ceramics at high temperature and in corrosive atmospheres for thermostructural applications is always limited by their low toughness. Fiber-reinforced ceramic matrix composites have been particularly promoted mainly for the aerospace industries. Indeed, damage in ceramic matrix composites (CMC) is characterized at the beginning by a progressive microcracking in the matrix.[1] According to discontinuities in the stresses at the matrix-cracks and the fiber–matrix interfaces, both the fibers and matrix must be able to move in order to fit the local stress field. It implies that the interfacial bond must be just weak enough to allow the debonding of the interface and the sliding of the fibers.

Glass and glass-ceramic matrix composites have been investigated by numerous works because they present the advantage, among others, of being fabricated at low temperature.[2–4] For wear applications, carbon fiber-reinforced matrix composites can be expected to present a low friction coefficient due to the possible lubricant properties of carbon fibers in some conditions.[5] Carbon fiber-reinforced YMAS glass-ceramic matrix composites have been fabricated for dry sliding applications.[6] In a first step, it was necessary to control the microstructural changes with temperature in the composites, the mechanical strength and crack propagation resistance, before beginning the tribological study. Indeed the behavior of materials in dry friction depends on many parameters like the test conditions and the geometry of the contacts. It depends also on the mechanical strength of the materials, on mechanical and physico-chemical reactions at the interface between both the parts in

contact, on the formation and the evolution of a third body in the contact.[7] This work[6,8] has led us to study in C/YMAS composites different behaviors according to the used carbon fiber and the thermal treatment applied for their processing. It has been shown that, as is well known nowadays for CMC,[9] these behaviors are closely related to interface properties. The required debonding energy and the average reloading stress—reloading of the matrix on both sides of the crack results from the stress transfer from fibers to the matrix, which is assumed to occur by shearing along the interface—are key parameters for CMC damage resistance. According to the magnitude of the shear stress τ, the interface will be named strong or weak. The stress τ depends at the same time on the friction coefficient, thermal stresses due to the thermal expansion mismatch between the fibers and the matrix, and on stresses induced by the Poisson's effects during mechanical tests. So, if the coefficient of thermal expansion (CTE) of the fiber (α_f) is lower than the CTE of the matrix (α_m), the fiber is submitted during the fabrication of the composites to a radial compression on cooling, and the fiber–matrix sliding is difficult. By contrast, if $\alpha_m - \alpha_f < 0$, the interface is submitted to tension which facilitates the extraction of the fibers.

For SiC/LAS composites,[10–14] it appears that the presence of a carbonaceous interphase contributes to composite strengthening by making easier sliding between the fiber and the matrix. The reactivity between a carbon fiber and silica, which is the predominant phase in the various glass matrix used for carbon fiber composites, has been studied by Benson *et al.*[15] At 1400°C, the contact between the carbon fiber and the matrix can lead to the formation of CO, CO_2 and SiO gases and solid reaction products, oxide or oxycarbide. Very adhesive interfaces with high shear stresses can be expected if the external mechanical pressure is sufficient to maintain the contact. Thermodynamic calculations show that the reaction between the carbon fiber and the matrix depends strongly on the presence of CO and CO_2 gases. Therefore, Tredway *et al.*[14] suggest the introduction of oxides in the matrix, like Nb_2O_5 or MoO_3, which can be reduced in carbides for very high pressures, in order to limit the reaction between silica and carbon.

The aim of this paper is to understand the role played by the fiber–matrix interface on the fracture behavior of C/YMAS composites. Two grades of fibers are used, so that the influence of their different properties, textures and chemical reactivity will have to be considered. This work had to precede the study of the tribological behavior composites, in order that it could take into account this influential parameter. Push-in tests are used to determine the interfacial shear strength and relate it to the different mechanical behaviors observed. The fiber–matrix interface of some composites is investigated by Transmission Electronic Microscopy (TEM) before mechanical testing.

2 Experimental Procedure

2.1 Composites

The YMAS (Y_2O_3, MgO, Al_2O_3, SiO_2) matrix is reinforced by unidirectional fibers. Two grades which differ from their precursor, pitch or PAN, and their properties, are used : the pitch-based carbon fiber P25 (AMOCO) and the PAN-based carbon fiber T400H (TORAYCA). Their main characteristics are summarized in Table 1. Their microstructure and texture have been widely described previously.[8] Cross-sections of Pitch-based carbon fibers exhibit a 'Pan-am' texture, with a conjunction of isotropic and anisotropic areas and a highly anisotropic but incomplete polyaromatic carbon skin. The cross-sections of the T400H fiber are characterized, like the PAN-based T300 grade from TORAYCA, by a coarsely isotropic texture with a local anisotropic radial texture in a ring at about one half or one third of the radius. Due to the dissimilar texture of T400H and P25 fibers, their coefficients of thermal expansion are different.[6]

The glass transition and crystallization temperature intervals of the YMAS matrix are, respectively, 815–855°C and 945–1055°C.[8,17]

Pre-preg sheets are prepared by using a slurry infiltration process of fiber tows. The impregnated fibers are wound on an hexagonal mandrel. The volumic fraction of fibers is nearly equal to 35%. After drying, cutting and debinding, the tapes are densified in argon by hot-pressing in the 950 to 1250°C temperature interval with a pressure of 10 MPa (LPA-DVM Goliath).[8,16]

Up to 1000°C, X-ray diffraction patterns[8,17] show that the matrix is mainly vitreous. The $MgAl_2O_4$ spinel precipitates above 1050°C, as well as the hexagonal high temperature cordierite and the α and β $Y_2Si_2O_7$ yttrium silicates. The SiO_2-Y_2O_3 system is very complex with many polymorphic phases in the case of $Y_2Si_2O_7$ (α, βb γ, δ).

Table 1. Characteristics of the fibers (given by the manufacturers)

Fiber	*P25*	*T400H*
Longitudinal tensile strength (MPa)	1400	4500
Longitudinal tensile modulus (GPa)	160	250
Tensile fracture elongation (%)	0·9	1·8
Density (g cm^{-3})	1·90	1·80
Diameter of the filaments (μm)	11	7

At 1250°C, the α-$Y_2Si_2O_7$ turns almost completely in the β form.

2.2 Mechanical tests

Three-point bend tests are performed on composites bars ($34\times6\times1{\cdot}5\,mm^3$) at room temperature, with a span 30 mm long and a loading rate of 0·2 mm min.[8,16] A displacement cell, set on the tension surface of the sample, in the middle, has allowed to obtain load-deflection curves.

2.3 Push-in test

The Vickers indentation equipment used is built on the base of an optical microscope equipped with two lenses and the indentation cell.[18] The sample is polished with a diamond powder suspension (grain size about 1 μm) and set up on a force cell which allows forces up to 1 N to be measured with an accuracy of 0·5 mN. Indentation have been realised in the middle of two crack phases and where the fiber distribution is homogeneous. The motorization of the microscope focusing permits to reach loading speeds varying between 2 and 50 mN s^{-1}. The minimum speed is used in order not to introduce any damage in surrounding fibers. The displacement of the indentor relative to the sample surface is measured with a capacitive cell, which gives a resolution of 10 nm for a 300 μm cell-sample surface distance. The load-indentor displacement curves are recorded by a computer (5 points per s).

2.4 Transmission electron microscopy

The micro- and nanotexture was studied with a transmission electron microscope (Philips CM12 TEM), using a 120 kV high voltage and a super-twin objective stage. The microscope was also equipped with an energy dispersive analysis of X-ray system (EDAX). Prior to TEM investigations, small pieces of composites were mechanically thinned on both sample faces using a dimple grinder (Gatan 656) with a diamond powder suspension (grains sizes were in the 2–4 μm range). Hence, ion-thinning was performed (Gatan Duomill 600) using a 4 kV high voltage and incidence angles from 20 to 12°.

Because of decohesion effects between fibers and matrices, embedding the composite samples in epoxy resin was often necessary to maintain the sample integrity during the thinning steps. The epoxy resin used (TAAB or POLARBED 812) was characterized by some content in chlorine. Any misinterpretation was then avoided by using the EDAX analysis.

A glassy ceramic matrix being an electrical insulator, the quality of the TEM images are not so good as with C/SiC composites.[19,20] Micrographs were then sometimes improved by using a very thin ($<$ 5 nm) carbon coating on the sample specimens for TEM.

3 Results

3.1 Fracture behavior

Pitch-based carbon fiber-reinforced YMAS composites have been hot-pressed.[8,17] Due to the thermal expansion mismatch between the carbon fibers (axial CTE $\approx 4{\cdot}5{\cdot}10^{-6\circ}C^{-1}$; radial CTE $\approx 15{\cdot}10^{-6\circ}C^{-1}$)[6] and the matrix (CTE $\approx 6{\cdot}10^{-6\circ}C^{-1}$),[8] thermal stresses are induced in the composites on cooling making a network of microcracks. Whatever the sintering temperature, the average distance between two microcracks is the same (about 250 μm), except for composites sintered at the highest temperature (1250°C) for which the distance can reach 1 mm. Fracture surfaces have shown fiber extractions about 1 mm long for composites sintered at 1250°C whereas, for the others, they are only about 100 μm long. The fracture of the composites is always controlled.

The mechanical behavior of T400H/YMAS composites is modified for each sintering condition. The ultimate strength varies from 300 to 1100 MPa for a 35% fiber volumic fraction. The average distance between microcracks, which have appeared on cooling in the composites due to the thermal expansion mismatch between the fibers (axial CTE $\approx 4{\cdot}10^{-6\circ}C^{-1}$; radial CTE $\approx 10^{-5\circ}C^{-1}$)[6] and the matrix, increases with sintering temperature. Up to 1150°C, the ultimate strength increases but the fracture remains brittle, except for the composite T1. In the case of brittle fractures, fiber extractions are about 100 μm long. For non-brittle fractures (T1), some bundles of fibers are easily pulled-out, due to their bad impregnation by the matrix at this sintering temperature.[8] For temperatures higher than 1150°C, the distance between cracks is increased again, the fracture strength decreases at the same time and the fracture tends to become less brittle. Fibers extractions are still about 100 μm long, but in delamination planes some bundles of fibers are easily and largely extracted.

In Table 2, the nomenclature used is summarized for the different composites with the hot-pressing conditions, the average distance between microcracks and the average fracture strength for a 35% fiber volumic fraction.[8]

3.2 Push-in results

A huge number of studies and models are devoted to the characterisation and properties of the fiber-matrix interfaces[21–24] in order to explain the fracture behaviour of ceramic–ceramic composites. The thermochemical analysis is based on debonding of the interface and the relative sliding of the fibers and the matrix which can be defined by the shear stress τ. In the case of C/YMAS composites,

Table 2. Main characteristics of P25/YMAS and T400H/YMAS composites,[8] interfacial debonding (σ_d) and shear (τ) stresses (for T400H fiber composites, the number of pushed fibers is indicated).

Ref.	*Densification conditions (°C-h)*	*Crystallisation conditions (°C-h)*	*Distance between microcracks (μm)*	*Fracture strength (MPa)*	*Fracture type*	σ_d *(MPa)*	τ *(MPa) (Number of pushed fibers)*
P1	950–1						
P2	970–1						
P3	1000–1						
P4	1050–0·5						
P5	1050–1		245 ± 65			455 ± 73	17·8 ± 4·8
P6	1050–1	1050–1·5		440 ± 60	Controlled		
P7	1050–1	1050–6					
P8	1100–1						
P9	1150–1						
P10	1050–0·5	1250–0·5	600 ± 180				
P11	1050–1	1250–1·5	1000 ± 270			59 ± 33	1·0 ± 0·7
T1	1000–1		95 ± 25	300 ± 45	Controlled	1322 ± 258	108 ± 33·7 [15]
T2	1025–1		100 ± 30	520 ± 70	Less controlled	1137 ± 167	36·3 ± 8·0 [6]
T3	1050–1		190 ± 35	670 ± 35			
T4	1100–1		330 ± 85	770 ± 105			
T5	1150–1		450 ± 120	1100 ± 300	Brittle	769 ± 285	16·7 ± 8·8 [20]
T6	1200–1		400 ± 110	760 ± 65			
T7	1050–1	1250–1·5	550 ± 150	570 ± 35	Less brittle	846 ± 162	20·4 ± 11·1 [9]

as is shown later, many parameters (thermal expansion, mismatch, matrix crystallisation, oxidation of the carbon fibers...) influence the fiber–matrix interface, so we have performed microindentation tests for a comparison and a quantitative study of the samples. In the case of continuous fiber composites, Marshall[25] was the first using a Vickers indentor to apply a load on a fiber (Nicalon) being perpendicular to the surface of a polished material. If the fiber–matrix bond is not too strong, the applied load is high enough to induce the sliding of the fiber in its matrix sheath.

The first part of an indentation curve corresponds to the elastoplastic response of the fiber, then the change of slope is related to debonding of the interface for the F_d force. If R is the radius of the fiber, the critical debonding stress can be expressed by the following equation:

$$\sigma_d = \frac{F_d}{\pi \cdot R^2} \tag{1}$$

The second part of the curve describes the relative fiber–matrix sliding. If the sliding is assumed purely frictional without shrinking of the interface, and if the deformation of the fiber under the load is neglected, the fiber–matrix reloading is carried out for a constant shear stress τ.[21]

To obtain an absolute value of the shear stress, it is necessary to take into account in this analysis other parameters such as the influence of the Poisson's effect under the indentation load which modifies the interfacial radial stress, the influence of the residual axial stress, the influence of the anisotropy of the fiber and the influence of the fiber roughness.[22–26]

If all these parameters are considered, the shear stress must not be supposed constant along the interface and the analysis becomes more complex.

The displacement cell measures the distance d between the indentor and the sample surface. It corresponds to the elastoplastic strain plus the fiber–matrix sliding, for forces higher than the debonding force F_d. Therefore, it is necessary, for valuing the shear stress τ, to determine, and extrapolate for forces higher than F_d, the elastoplastic strain according to the law $h = \alpha \cdot F^{\beta}$. Then the fiber–matrix sliding u is obtained by subtracting the elastoplastic strain h to the measured displacement d, and the shear stress can be extracted from the following relation(2):

$$\forall F \geq F_d, \tau = \frac{F^2 - F^2 d}{4 \cdot \pi^2 \cdot R^3 \cdot E_f \cdot u} \tag{2}$$

Experimental load-indentor displacement curves with the corresponding elastoplastic curves are represented in Fig. 1 where different debonding and sliding behaviors are shown. For the P5 composite, the force required for debonding is higher than for P11, for which afterwards sliding is easier. These experiments have been reproduced six times for each composite. Statistical debonding and sliding stresses are summarized in Table 2. They confirm that the strength of the interface is very low for the composite P11, which agrees with previous observations on the pull-out lengths on surface fractures and the increase of the distance between microcracks. The distance between cracks is inversely proportional with the interfacial shear stress.[1] A low interfacial shear stress

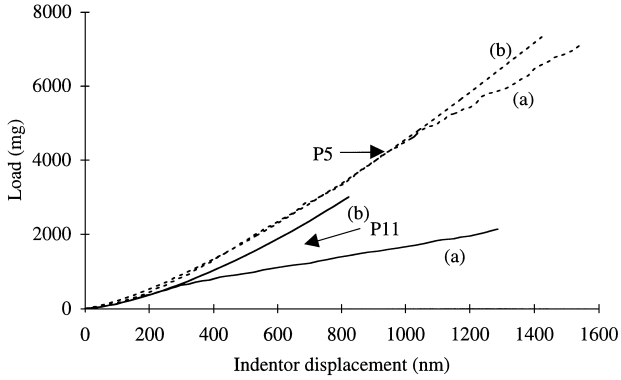

Fig. 1. Experimental load-indentor displacement and associated elastoplastic curves for P5 and P11 composites.

corresponds to a weak interface which allows the sliding of the fibers in matrix blocks and their easier extraction.

In the same way, indentations are realised on composites containing T400H fibers. Average debonding and sliding stresses are summarized on Table 2 with the number of indented fibers. These results allow a general trend to be defined. The σ_d and τ stresses decrease when the sintering temperature is raised up to 1150°C, which is in agreement with the changes in ultimate strengths and distances between microcracks but also with TEM observations of the fiber–matrix interface, as will be explained later. For T5 and T7 composites, debonding and sliding stresses are nearly similar, in the same way as fiber extraction lengths except in delamination planes. Thus the lower fracture strength and the more controlled fracture for T7 would be due to this delamination.[8]

3.3 Observation of the fiber–matrix interface and discussion

The P25 fiber presents statistically a 'Pan-Am' cross-sectional texture with a highly anisotropic but uncomplete graphite-like carbon skin, which does not adhere well to the fiber; such a skin, if any, is made of polyaromatic layer stacks, exhibiting few structural defects, and often lying flat on the fiber surface. The fiber surface may appear either smooth or corrugated (Fig. 2).[8]

Highly corrugated fibers [Fig. 2(b)] are associated with high concentrations of isotropic areas in the outer zone of the fibers. These areas (light areas in the picture) are often found altered (oxidized), and not associated with graphite-like flakes nor interfacial separations. On the contrary, for the smooth fibers [Fig. 2(a)], debondings are more obvious, while pieces of graphite-like flakes do not adhere to the fiber and are often found on the matrix side of the debonding, sometimes embedded within the matrix. Such discrepancies in outer isotropic zone concentrations are assumed to originate from the preparation conditions, specifically a lack of control of the phase distribution within the precursor, which is a two-phase petroleum pitch.

The poorly organised carbon in the isotropic areas exhibits a higher reactivity regarding the matrix compared to the graphite-like flakes lying flat on the fiber. Indeed, it has been shown that the edge atoms in graphitic structures are more reactive than basal atoms[31] and the study of carbon reactivity is now grounded on the active site concept.[32] Depending on the time/temperature conditions, the reactivity may induce chemical bondings, when limited, or carbon gasification, when extensive. Partial oxidation of some fibers during the composite preparation could thus lead to some alteration of the isotropic areas close to the fiber surface, as observed. On the contrary the outer graphite-like skin, when any, could prevent the fiber from oxidation by the matrix to some extent.

Whatever the sintering conditions are, the debondings are very often localized between the stiff carbon layers of the graphite-like flakes and the rest of the fiber (Figs 3 and 4). This feature often links the fiber and the matrix one to each

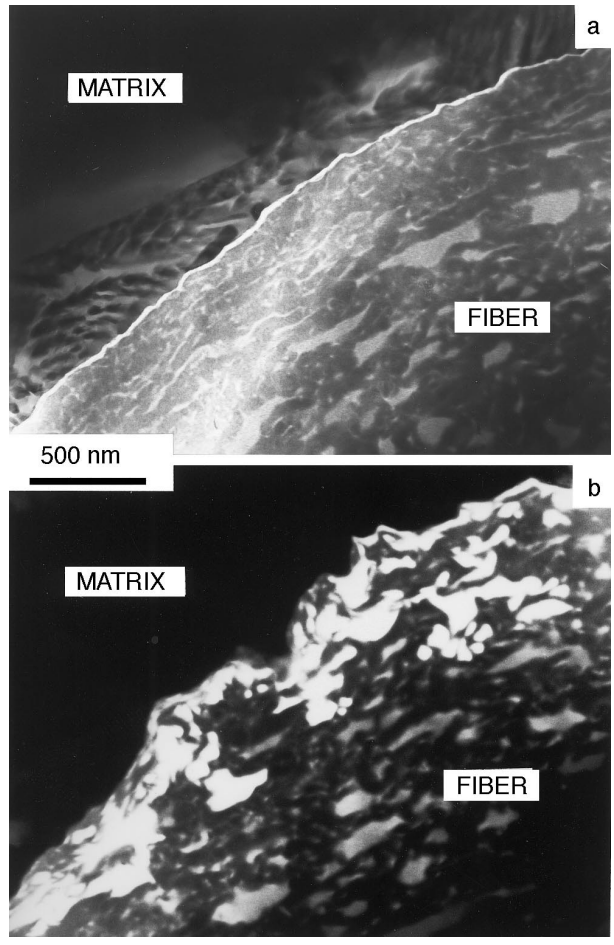

Fig. 2. Composite P5. Bright field TEM images, cross-section. Light areas within fibers are isotropic parts.[8] (a) and (b) are two examples of P25 fibers with various corrugated surfaces. The bright rim at the interface indicates a fiber–matrix decohesion.

other through the graphite-like flakes (Fig. 4). In some cases [P3 or P5, Fig. 2(a)], the outlines of the matrix may follow rather well those of the fiber, which indicates specifically that the debondings are mainly due to the thermal expansion mismatch between both constituents. On the other hand, for other composites, the outlines on both sides of the debonding are not parallel, which suggests that debonding is not due to the thermal expansion mismatch only. Other reasons could be a poor wettability of the fiber surface by the glassy matrix when the hot-pressing time is too short (P10, Fig. 5), or some gasification due to oxydo-reduction reactions with the matrix when an annealing is performed at high temperature (P10 or P11) for a long time (P7, Fig. 6). Indeed, the amorphous aspect of several fiber–matrix contact zones supports a possible matrix reduction effect, as far as the partial oxidation of polyaromatic carbon can lead to the destruction of its structural organization and to a polyaromatic carbon phase without any evident texture.[33] It is noteworthy that the high anisotropy of the graphite-like carbon flakes prevents them from being oxidised by the matrix, and that oxidized carbon is found behind the flakes, i.e. between the flakes and the bulk fiber (Fig. 7).

From the microcrack examination, the indentation experiments (Table 2), and the TEM study, it is possible to state that interfacial debonding can issue from four origins : (1) the thermal expansion mismatch between the fiber and the matrix, (2) the matrix shrinkage due to structural changes such as glass/crystal transformation or phase changes, (3) the poor wettability due to the high viscosity of the glass, and (4) the oxidation of carbon fibers by the

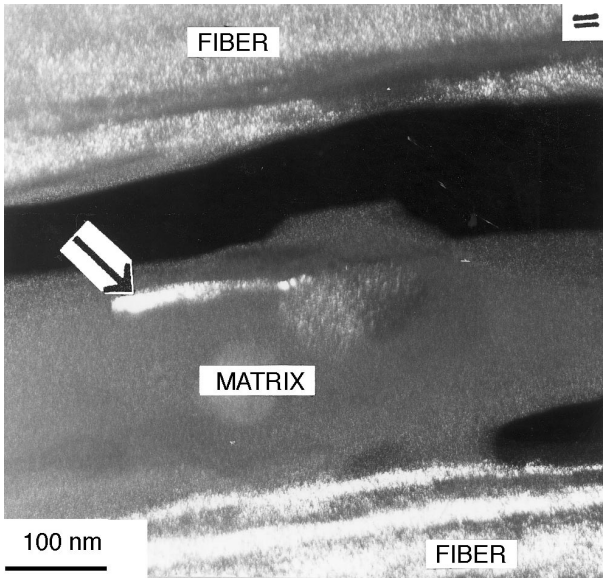

Fig. 3. Composite P3. C_{002} dark field TEM image, longitudinal section. Bright areas are due to graphenes layers oriented parallel to the double bar sign. The bright rim (arrow) into the matrix is part of a graphite-like flake surrounded then embedded by the glass.

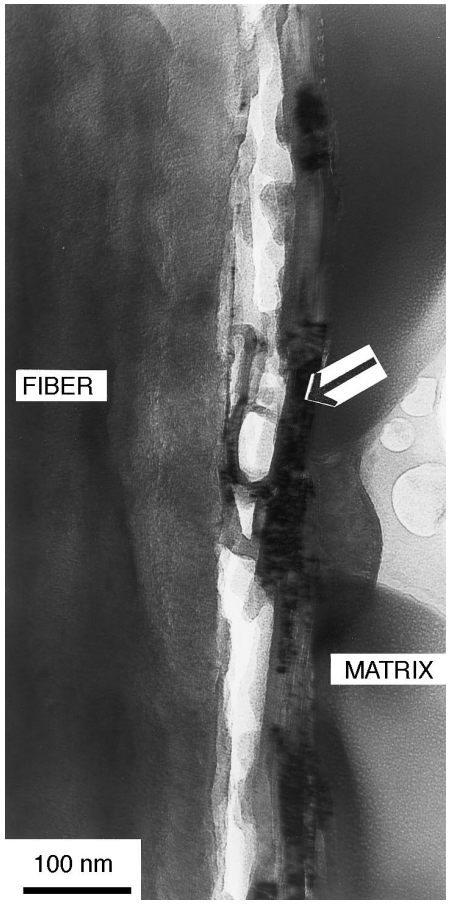

Fig. 4. Composite P11. Bright field TEM image, longitudinal section. The fiber–matrix decohesion occurs between the graphite-like flake (arrow) and the fiber, as in Figs 3 and 7.

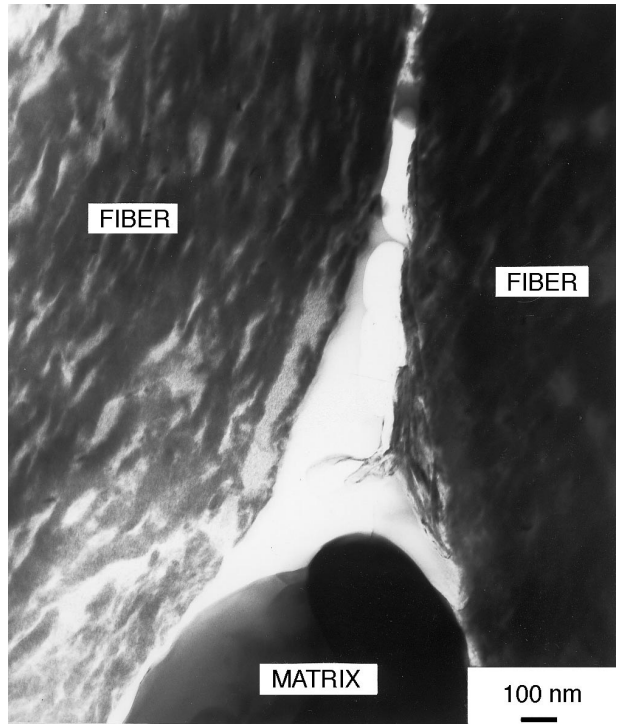

Fig. 5. Composite P10. Bright field TEM image, cross-section. Example of the poor wettability of the fibers by the matrix due to the high viscosity of the glass associated with a short densification time.

matrix (without formation of any carbide). The relative importance of the four reasons depends on the sintering conditions. Effect of reason (1) (thermal expansion mismatch) increases with the densification plus crystallization temperature, effect of reason (2) (matrix shrinkage) is high from the crystallization temperature (1100°C)[17] but more limited afterwards, effect of reason (3) (poor wettability) is high for short densification times, effect of reason (4) (carbon gasification) increases with densification plus crystallization temperature or time.

T1 composite was the one exhibiting the highest porosity (15%), making it very friable so that cross-sections were not possible to prepare. Therefore, the quality of the fiber–matrix interface was not able to be accurately characterized. However, from TEM observations (Fig. 8), it is unlikely that the porosity is mainly located in interfacial zones.

On the contrary, an interfacial separation about 30 nm wide is observed on a cross-section of the T5 composite (Fig. 9). The debonding is essentially due to the thermal expansion mismatch between the fibers and the matrix (parallel outlines). However some contact zones are detected.

In the interfacial contact zones, both for T1 or T5, the carbon is highly disordered (Fig. 10). This amorphous-like carbon interphase, about 20 nm thick, may be due to the oxidation of the fiber surface by the matrix but can also originate from the pyrolysis and carbonization of sizing. Sizing is about 30 nm thick[34] and its carbonization can have led to a 15 nm thick carbonaceous residue.

For the T6 composite, the pressure is applied at 1200°C, i.e. at a temperature where the matrix viscosity has become too high for a good wettability (Fig. 11) of the fibers by the matrix due to the progress of the crystallisation as shown by XRD experiments.[8]

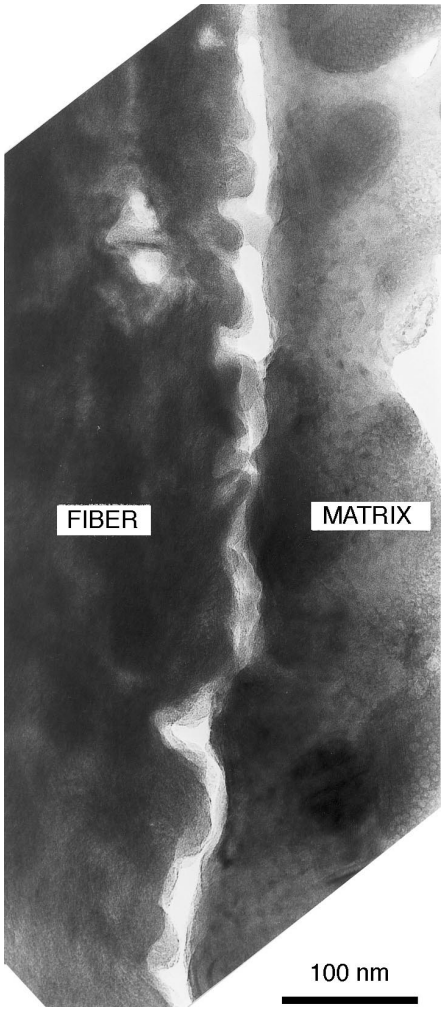

Fig. 6. Composite P7. Bright field TEM image, cross-section. The matrix surface outline does not match well the fiber surface, possibly due to the partial oxidation of the fiber enhanced by the high temperature/time densification conditions.

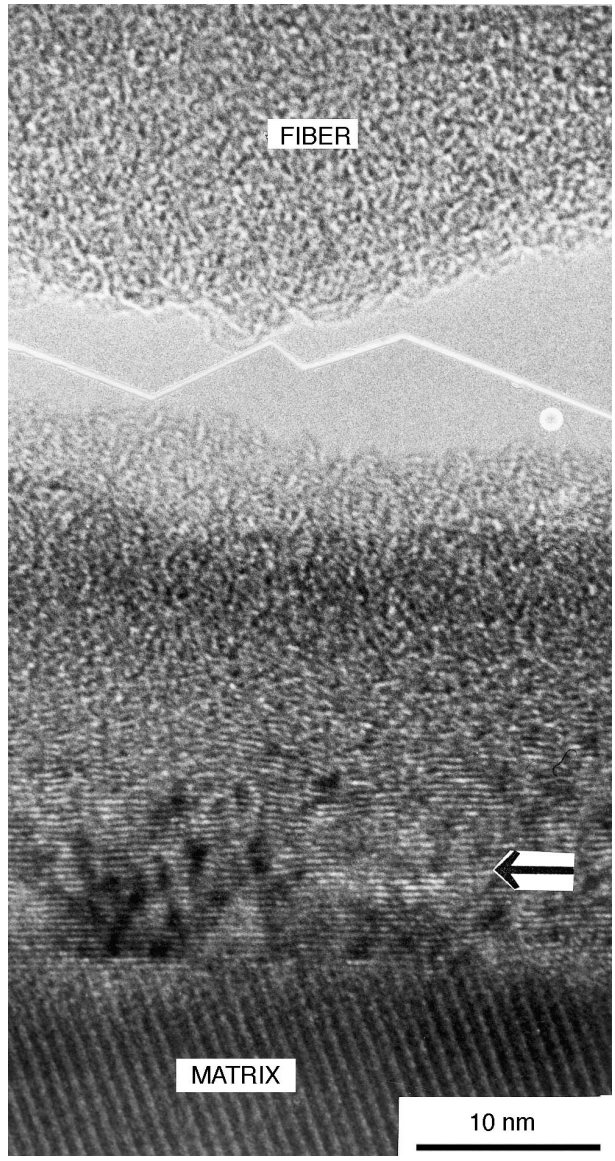

Fig. 7. Composite P11. Lattice fringe TEM image, cross-section. Again, the decohesion occurs between the graphite-like flake (arrow) and the fiber. The actual decohesion width is 25–30 nm. The fiber surface is altered by oxidation (the graphene fringe cannot be image) while the graphite-like flake (arrow) is not, though at the very contact to the matrix.

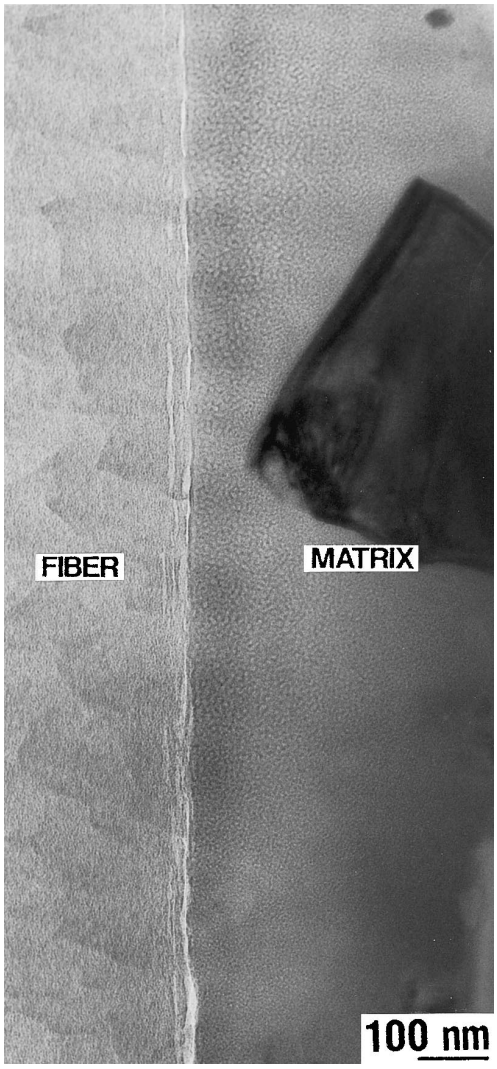

Fig. 8. Composite T1. Bright field TEM image, longitudinal section. Since not diametral, such a section is not suitable to evidence interfacial decohesion, however, it is doubtful that the 15% porosity are located at interfacial areas.

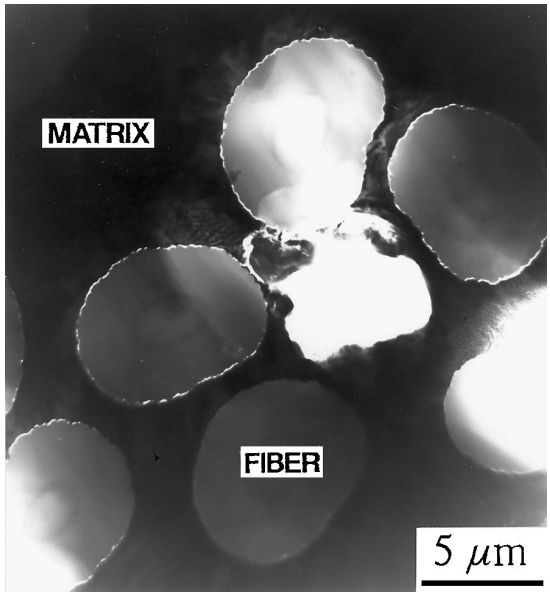

Fig. 9. Composite T5. Bright field TEM image, cross-section. Decohesions occur at the fiber–matrix interfaces, though some contact zones are found. Fiber and matrix outlines match rather well.

For the T7 composite, the interfacial separation is slightly wider, on average 100 nm. The outlines of the matrix are very often different from those of the fiber (Fig. 12). Nevertheless, some contact zones, where carbon is amorphous-like, revealing a strong alteration, always subsist.

The same four reasons already discussed above for the P25-reinforced composites are able to account for the differences in interfacial features within the T400H-reinforced composites. The thermal expansion mismatch, though effective, is less important because the radial CTE of the

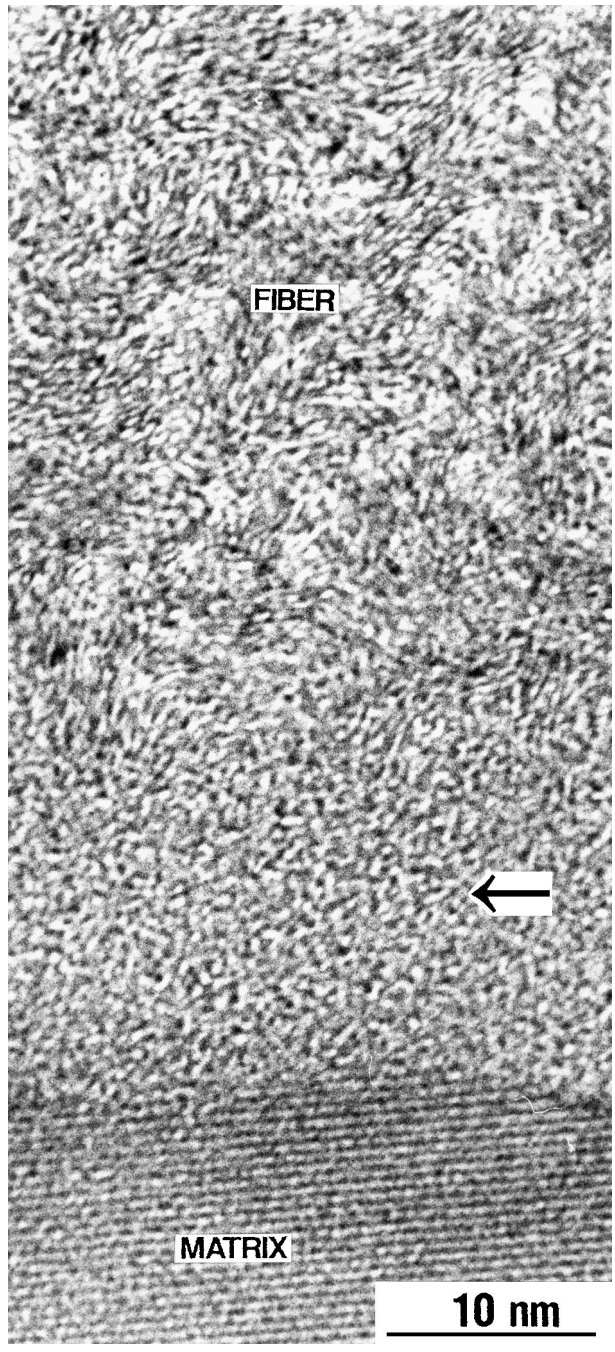

Fig. 10. Composite T5. Lattice fringe TEM image, cross-section. Occurrence of an amorphous carbon zone (arrow) at the points of fiber–matrix contact, either due to the oxidation of the fiber surface or possibly to the carbonisation of the polymer sizing.

T400H fiber is lower than that of P25 fibers (see Section 3·1). Actually, interfacial decohesions are less important for all of the T400H-reinforced composites compared to P25-reinforced composites. This has helped in maintaining fiber–matrix contact areas in all of the T-type composites, which are the sites of fiber–matrix chemical interactions. Depending on the hot-pressing conditions, the contact zones are more or less numerous, and depending on the ultimate temperature used, the chemical interactions may have a positive (bonding) or negative (gasification effect) on the interface strength. Finally, two main differences are that, during the thermal treatment (densification or crystallization), gaseous nitrogen (originating from the PAN precursor) is released from T400H fibers, and that the sizing of the fibers is likely to carbonize into a thin amorphous-like carbon phase.

Thus for T-400 H-reinforced composites, T1 composite exhibits a low fracture strength with a high interfacial shear stress but a controlled fracture, which is possibly the resulting effect of both a relatively strong fiber–matrix bonding through a poorly organized interphase (which induces high τ values and a low fracture strength) together with the high porosity mainly due to the N_2 release (which leads to a controlled fracture because of a bad impregnation of some bundles of fibers). From T1 to T5, the N_2 release is less and less important at the hot-pressing step, therefore less and less disturbing for the fiber–matrix contact, while the fiber–matrix chemical interactions are closer to an alteration process, making the interfacial shear stress weaker. T7 composite exhibits mechanical features similar to those of T1, i.e. a low fracture strength and a controlled fracture. The fact that the sintering temperature range (1050°C) was corresponding to the largest N_2 release together with a good fluidity of the matrix, and also the fact that the high crystallization temperatures (1250°C) was able to alter the carbon interfacial zones, could lead to local great fiber–matrix debondings. More generally, moderate τ values have been measured and comparatively short extractions observed, except in delamination planes.

Finally, T5 composite appears as the convenient compromise, with a hot-pressing temperature (1150°C) sufficiently low not to reach the complete matrix crystallization, sufficiently high to allow most of the gaseous N_2 to be released before

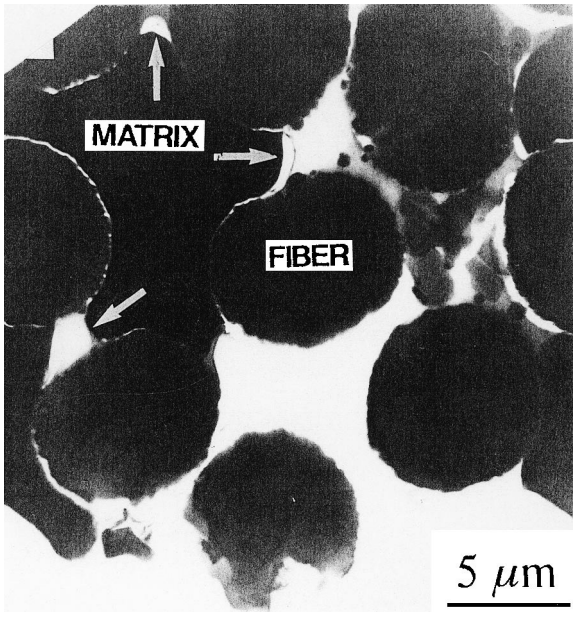

Fig. 11. Composite T6. Bright field TEM image, cross-section. Example of the poor wettability of the fibers by the matrix, due to the high viscosity of the matrix associated with a high densification temperature, which enhances the recrystallisation progress.

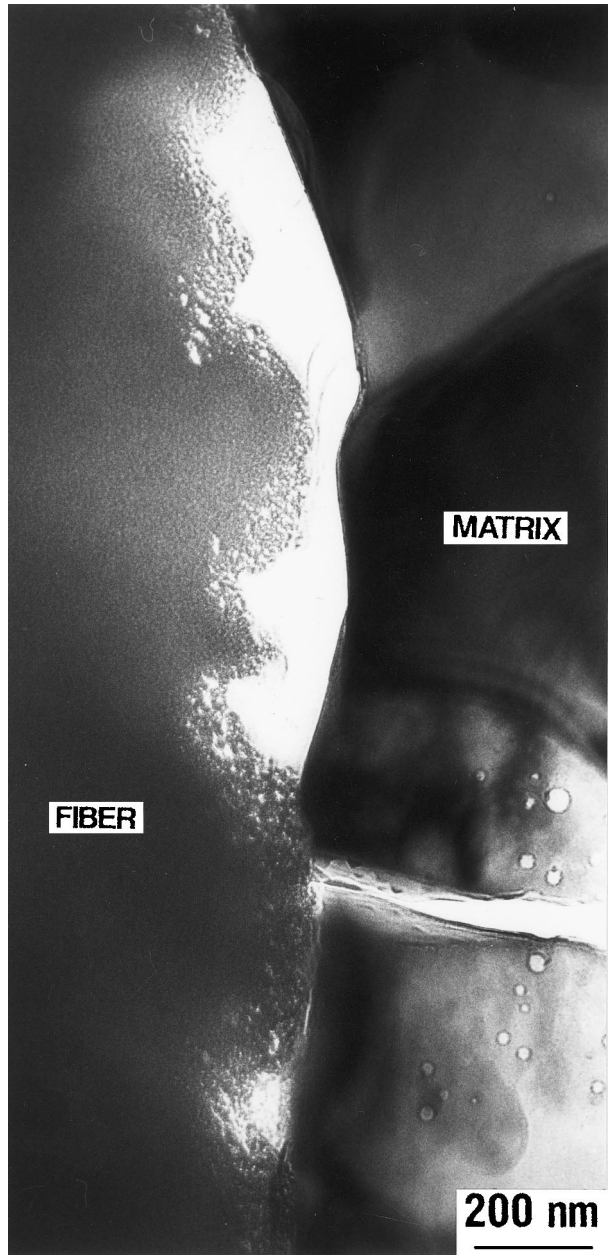

Fig. 12. Composite T7. Bright field TEM image, cross-section. The fiber surface outline does not match well the matrix outline, due to a conjunction of events such as high gaseous nitrogen release and crystallisation of the matrix.

applying the pressure, and sufficiently moderate to allow non-drastic carbon oxidation reactions to occur. Correspondingly, the fracture strength is highest with a rather brittle fracture.

4 Conclusion

The chemical reactivity of carbon fiber-reinforced YMAS composites depends strongly on the carbon fibers used and the hot-pressing conditions which influence the nature and the strength of the fiber–matrix interface.

The P25 pitch-based fibers are characterized by a highly anisotropic but uncomplete graphite-like carbon skin, which does not adhere well to the fibers, so that the debondings are very often localized between the stiff carbon layers and the rest of the fibers. Due to this interfacial separation, the interfacial shear stress is always relatively low and the sliding is then made possible. Consequently, the fracture is always controlled and the ultimate strength of all the composites in the same order of magnitude. However, the preparation of composites at high temperature (1250°C) seems to lead to a predominant effect of the oxidation of the carbon fibers by the matrix with some residual amorphous-like contact zones.

The mechanical behaviour of PAN-based carbon fiber-reinforced composites is more sensible to hot-pressing conditions, due to several mechanisms which can have opposite effects. The strength of the fiber–matrix bonds depends on the quality of the amorphous-like carbon interphase, which may proceed from the carbonization of sizing or may be due to the oxidation of the fiber surface by the matrix. The interfacial shear stress is high for sintering at low temperature because the interphase is not altered and the bond is strong. For higher hot-pressing temperatures, the shear stress decreases, allowing dissipation of much energy by debonding and sliding, and thus the improvement of the fracture strength. A high crystallisation of the matrix prevents the fibers from a good wetting, but also accentuates the effect of oxidation which, added to change N_2 releases, leads to local debondings. The ultimate strength is then lowered but the fracture is more controlled.

The aim of this work was to relate, precisely, the nature and the strength of the interface to the macroscopic behavior of composites. The importance of the thermal expansion mismatch between both constituents has not yet been entirely discussed and is the subject of a separate paper[35] when a synthesis between the role played by the thermal residual stresses and the chemical reactivity of both constituents is realised.

References

1. Aveston, J., Cooper, G. A. and Kelly, A., The properties of fibre composites: strength and toughness in fibre reinforced ceramics. In *Conference Proceedings*, National Physics Laboratory, Teddington, 1971, pp. 63–73.
2. Sambell, R. A. J., Briggs, A., Phillips, D. C. and Bowen, D. H., Carbon fibers composites with ceramic and glass matrices, Part 2, Continuous fibers. *J. Mater. Sci.*, 1972, **7**, 676–81.
3. Prewo, K. M. and Brennan, J. J., High strength silicon carbide fiber-reinforced glass matrix composites. *J. Mater. Sci.*, 1980, **15**, 463–68.
4. Seraudie, C., Elaboration et propriétés thermomécaniques de composites à fibres de carbure de silicium et matrices vitrocéramiques. Ph.D. thesis, Limoges University, 1995.
5. Hutchings, I. M., Tribology : Friction and Wear of Engineering Materials. Edward Arnold, London, Melbourne, Auckland, 1992.
6. Bianchi, V., Composites à fibres de carbone et matrice YMAS : elaboration, microstructure, comportements mécanique et tribologique. Ph.D. thesis, Limoges University, 1995.
7. Berthier, Y., Tribologie, Science Carrefour. In *Journeé Européenne du Freinage*, JEF 92, GFC 92 Lille, 1992.
8. Bianchi, V., Sinkler, Goursat, P. W., Monthioux, M. and Ménessier, E., Carbon fiber-reinforced (YMAS) glass-ceramic matrix composites. I. preparation, structure and fracture strength. *J. Europ. Ceram. Soc.*, accepted.
9. Kerans, R. J., Hay, R. S., Pagano, N. J. and Parthasarathy, T. A., The role of the fiber-matrix interface in ceramic composites. *Am. Ceram. Soc. Bull.*, 1989, **68**, 429–442.
10. Brennan, J. J., Interfacial characterization of glass and glass-ceramic matrix/Nicalon SiC fiber composites. Tailoring multiphase and composite ceramics. *Mater. Sci. Res.*, Vol. 20 ed. R. E. Tressler, G. L. Messing, C. G. Pantano and R. E. Newham. Plenum Press, New York, 1986, pp. 549–560.
11. Bleay, S. M., Scott, V. D., Harris, B., Cooke, R. G. and Habib, F. A., Interface characterization and fracture of calcium aluminosilicate glass-ceramic reinforced with Nicalon fibres. *J. Mater. Sci.*, 1992, **27**, 2811–2822.
12. Prewo, K. M., Carbon fibre reinforced glass matrix composites tension and flexure properties. *J. Mater. Sci.*, 1988, **23**, 2745–2752.
13. Benson, P. M., Spear, K. E. and Pantano, C. G., Interfacial characterization of glass matrix/Nicalon SiC fiber composites : a thermodynamic approach. *Ceram. Eng. Sci. Proc.*, 1988, **9**, 663–669.
14. Tredway, W. K., Prewo, K. M. and Pantano, C. G., Fiber matrix interfacial effects in carbon fiber-reinforced glass matrix composites. *Carbon*, 1989, **27**, 717–727.
15. Benson, P. M., Spear, K. E. and Pantano, C. G., Thermomechanical analyses of interface reactions in carbon-fiber-reinforced glass matrix composites. *Mater. Sci. Res.*, 1987, **21**, 415–425.
16. Bianchi, V., Goursat, P., Ménessier, E., Sinkler, W. and Monthioux, M., C/YMAS composites—effects of the interface and the residual stresses on the rupture behavior. In *Advanced Structural Fiber Composites, Advances in Science and Technology*, Vol. 7, 1994, pp. 695–702.
17. Sinkler, W., Monthioux, M., Bianchi, V., Goursat, P. and Ménessier, E., Carbon fiber-reinforced YMAS glass-ceramic matrix composites. II: Structural changes in the matrix with temperature. *J. Europ. Ceram. Soc.*, 1995, submitted.
18. Parlier, M., Passilly, B. and Sudre O., Caractérisation micromécanique dees composites à matrice céramique à l'aide de la technique de microindentation instrumenteé. In *Workshop II: Introduction of Ceramics in Aerospace Structural Composites, 76th Meeting of the Structures and Materials Panels*, Anthalya, Turkey, 1993.

19. Després, J. F. and Monthioux, M., Mechanical properties of C/SiC composites as explained from their interfacial features. *J. Eur. Cer. Soc.*, 1995, **15**, 209–224..
20. Grathwohl, G., Hämel, A., Meier, B., Pippel, E., Richter, G. and Wolterdorf, J., Fibre-reinforced SiC-matrix composites:microstructure, interfaces and mechanical properties. *J. Eur. Cer. Soc.*, 1992, **10**, 1–12.
21. Marshall, D. B., An indentation method for measuring matrix fiber frictional stresses in ceramic composites. *J. Am. Ceram. Soc.*, 1984, **67**, C259.
22. Sigl, L. S. and Evans, A. G., Effects of residual stress and frictional sliding or cracking and pullout in brittle matrix composites. *Rech. Materials*, 1989, **8**, 1–12.
23. Bright, J. B., Shetty, D. K., Griffin, C. W. and Limaye, S. Y., Interfacial bonding and friction in silicon carbide (filament) reinforced ceramic and glass-ceramic composites. *J. Am. Ceram. Soc.*, 1989, **72**, 1891–1898.
24. Hutchinson, J. W. and Jensen, H. M., Models of fiber debonding and pullout in brittle composites with friction. *Mechanics of Materials*, 1990, **9**, 190–163.
25. Marshall, D. B. and Oliver, W. C., Measurement of interfacial mechanical properties in fiber-reinforced ceramic composites. *J. Am. Ceram. Soc.*, 1987, **70**, 542–548.
26. Hsueh, C. H., Ferber, M. K. and Wereszczak, A. A., The relative residual fibre displacement after indentation loading and unloading of fibre-reinforced ceramic composites. *J. Mater. Sci.*, 1993, **28**, 2227–2232.
27. Hsueh, C. H., Evaluation of interfacial properties of fiber-reinforced ceramic composites using a mechanical properties microprobe. *J. Am. Ceram. Soc.*, 1993, **76**, 3041–3050.
28. Hsueh, C. H. and Ferber, M. K., Evaluation of residual axial stresses and interfacial friction in Nicalon fibre-reinforced macro-defect-free cement composites. *J. Mater. Sci.*, 1993, **28**, 2551–2556.
29. Hsueh, C. H., Interfacial debonding and fiber pull-out stresses of fiber-reinforced ceramic composites. IX : A simple treatment of Poisson's effect for frictional interfaces. *Mater. Sci. Eng.*, 1993, **A161** L1.
30. Zhou, L. M. and Mai, Y. W., On the single fibre pull-out and push-out problem : effect of fibre anisotropy. *Z. Angew Math. Phys.*, 1993, **44**, 769–775.
31. Laine, N. R., Vastola, F. J. and Walker, P. L., The importance of active surface area in the carbon-oxygen reaction. *J. Phys. Chem.*, 1963, **67**, 2030–2035.
32. Donnet, J. B., Structure and reactivity of carbons : from carbon blocks to carbon composites. *Carbon*, 1982, **20**, 267–282.
33. Cojean, D. and Monthioux, M., Unexpected behavior of interfacial carbon in SiC.SiC composites during oxidation. *Br. Ceram. Trans. J.*, 1992, **91**, 188–196.
34. Le Coustumer, P., Lafdi, K. and Oberlin, A., Imaging of sizing upon carbon fibers. *Carbon*, 1992, **30**, 1127–1133.
35. Bianchi, V., Goursat, P. and Ménessier, E., Carbon fiber-reinforced (YMAS) glass-ceramic matrix composites. IV. Thermal residual stresses and fiber/matrix interfaces. *Composite Science and Technology*, in press.